Design and Synthesis of Inhibitors of *Plasmodium falciparum* *N*-Myristoyltransferase, A Promising Target for Antimalarial Drug Discovery

Zhiyong Yu,[†] James A. Brannigan,[‡] David K. Moss,[§] A. Marek Brzozowski,[‡] Anthony J. Wilkinson,[‡] Anthony A. Holder,[§] Edward W. Tate,*[,†] and Robin J. Leatherbarrow*[,†]

[†]Department of Chemistry, Imperial College London, London SW7 2AZ, U.K.
[‡]York Structural Biology Laboratory, Department of Chemistry, University of York, York YO10 5DD, U.K.
[§]Division of Parasitology, MRC National Institute for Medical Research, The Ridgeway, Mill Hill, London NW7 1AA, U.K.

S *Supporting Information*
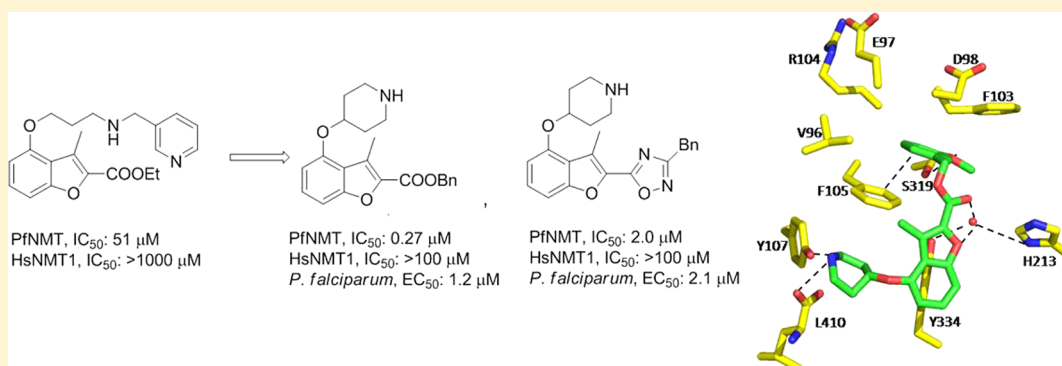
ABSTRACT: Design of inhibitors for *N*-myristoyltransferase (NMT), an enzyme responsible for protein trafficking in *Plasmodium falciparum*, the most lethal species of parasites that cause malaria, is described. Chemistry-driven optimization of compound **1** from a focused NMT inhibitor library led to the identification of two early lead compounds **4** and **25**, which showed good enzyme and cellular potency and excellent selectivity over human NMT. These molecules provide a valuable starting point for further development.

■ INTRODUCTION

Malaria, a disease caused by protozoan parasites of the genus *Plasmodium*, is a demanding health problem. The most lethal form, caused by *Plasmodium falciparum*, was responsible for nearly 655000 deaths in 2010, mainly of children below the age of five.[1] Although recent vaccine trials are giving promising results,[2] chemotherapy remains the mainstay of antimalarial treatment. Since chloroquine has lost its efficacy in most endemic areas due to the rapid development of drug resistance,[3] artemisinin-based combination therapies serve as the current gold standard.[4] Recently, signs of emerging resistance to artemisinins[5] have led to renewed efforts to develop novel antimalarial agents, with purely synthetic tri/tetraoxane and spiroindolone among the most promising candidates.[6−10]

The enzyme *N*-myristoyltransferase (NMT) represents a promising drug target[11] because it has been shown to be essential in many organisms.[12−15] NMT, a monomeric enzyme ubiquitous in eukaryotes, catalyzes an irreversible cotranslational or posttranslational transfer of myristate (C14:0 fatty acid) from myristoyl-coenzyme A (myr-CoA) to the *N*-terminal glycine of a subset of eukaryotic proteins.[16,17] Although genetic knockdown of NMT in *P. falciparum* has yet to be achieved presumably

due to its essentiality, myristoylated proteins such as glideosme-associated protein-45, ADP-ribosylation factor-1, and calcium-dependent protein kinase-1 have been characterized and shown to be critical for parasite viability.[18−21] Furthermore, a novel inducible knockout of NMT in the closely related mammalian pathogen *Plasmodium berghei* has demonstrated an acute dependence on NMT activity in the parasite life cycle.[22] It seems likely that inhibition of myristoylation also has an equal potential to disrupt key biological pathways in *P. falciparum*.

N-Myristoylation by NMT follows an ordered Bi−Bi mechanism in which the binding of myr-CoA to NMT occurs prior to the protein substrate.[23] Binding of myr-CoA facilitates the opening of a second pocket, to which the protein substrate binds. Transfer of myristate to the protein substrate takes place via a nucleophilic addition−elimination reaction, and this is followed by ordered release of CoA and the myristoylated protein. In contrast to the myr-CoA pocket, which is highly conserved across species, the peptide binding cavity is more divergent.

As a result, inhibitors of fungal NMTs have been discovered by several research groups that are competitive with the protein substrate and show excellent selectivity relative to human NMT.[24−29]

A "piggy-back" approach[30] was used to identify compound **1** (Figure 1) as a hit by screening a focused library of reported

IC$_{50}$ PfNMT: 51 μM
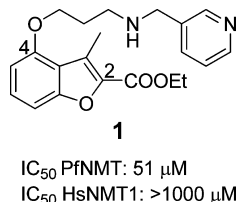IC$_{50}$ HsNMT1: >1000 μM

Figure 1. Structure and biological activity of compound **1**.

Candida albicans NMT (CaNMT)[24−29] and *Trypanosoma brucei* NMT (TbNMT) inhibitors.[31,32] Compound **1**, initially developed by Roche in an antifungal campaign,[29] showed moderate inhibition against PfNMT and promising selectivity over human NMT1 (HsNMT1).

Herein we report the design of potent and selective *P. falciparum* NMT (PfNMT) inhibitors based on the structure of compound **1**. Crystal structures of NMT inhibitors enabled experimentally derived structure−activity relationships (SAR) to be interpreted, and mutagenesis studies provided a rational basis for human enzyme selectivity.

■ RESULTS AND DISCUSSION

Investigation of the *C*-4 Side Chain. In the absence of structural information for *Plasmodium* NMT at that time, a chemistry-driven approach was adopted. On the basis of the structure of compound **1**, *C*-4 and *C*-2 side chains were identified as promising sites for modification (Figure 2). Exploration of 24 variations in the *C*-4 side chain revealed SAR, which are similar to those Roche found in their CaNMT project:[24] (i) trimethylene is an optimal chain length, (ii) a secondary amine X is preferred (Tables S1−S3, Supporting Information). Conformational restriction of the trimethylene side chain by replacement with 4-piperidinol resulted in the discovery of compound **2** (Figure 2). **2** showed 3-fold activity improvement over **1** while maintaining good human selectivity. In addition, **2** is more druglike than **1** in terms of lower molecular weight, fewer rotatable bonds, and is also more synthetically tractable. Therefore, 4-piperidinol was considered to be an optimal *C*-4 side chain. More importantly, this compound also displayed moderate antiparasitic activity, with an EC$_{50}$ value of 15 μM.

Investigation of the *C*-2 Side Chain. The study of the *C*-2 side chain began by varying the R^2 group of the ester and replacement of the latter by an amide (Scheme 1). An *N*-Boc piperidinol side chain was incorporated into the readily synthesized benzofuran scaffold[33] via a Mitsunobu reaction, followed by hydrolysis of the ethyl ester to form the key intermediate **I-2**. The ester and amide with different R^2 groups were synthesized under standard coupling conditions (Table 1). Larger R^2 groups, especially those including an aromatic ring
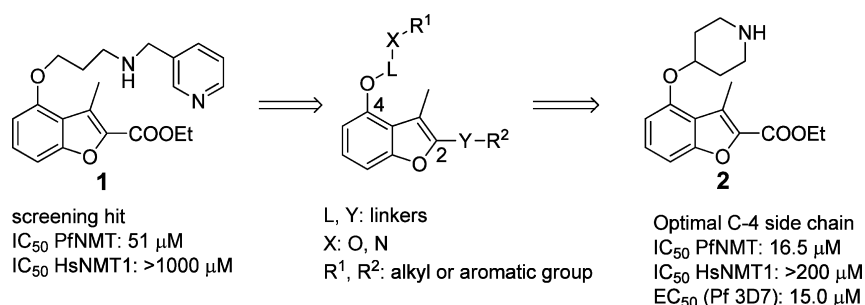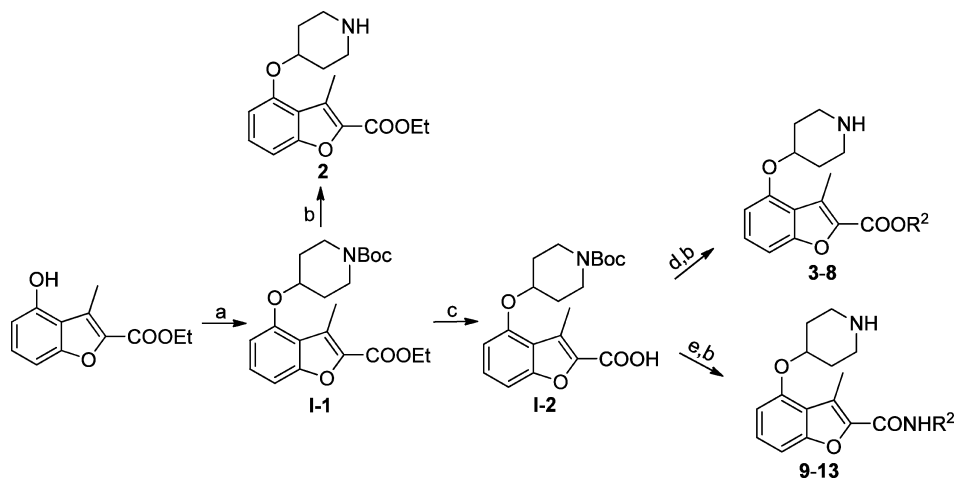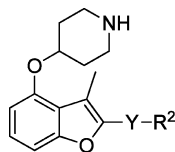

Figure 2. Modification of *C*-4 side chain of compound **1**.

Scheme 1[a]

[a]Reagents: (a) DIAD, PPh$_3$, *N*-Boc-4-OH piperidine, THF, rt, 4 h, 95%; (b) 5% TFA in DCM, rt, 2 h, quantitative; (c) LiOH, MeOH/H$_2$O, 50 °C, 4 h, 90%; (d) EDCI, HOBt, DIPEA, R^{2}OH, CH$_3$CN, rt, 4 h, 70−90%; (e) PyBOP, DIPEA, R^{2}NH$_2$, DMF/DCM, rt, 3 h, 50−70%.

Table 1. Activities of Esters and Amides against PfNMT[a]

compd no.	Y	R^2	IC_{50} (μM)	compd no.	Y	R^2	IC_{50} (μM)
2	COO	Et	16.5	8	COO(CH$_2$)$_3$	Ph	36.2
3	COO	Ph	24.4	9	CONH	i-Pr	>200
4	COOCH$_2$	Ph	0.27	10	CONH	cyclo-hex	>100
5	COOCH$_2$	α-napthyl	1.4	11	CONH	Ph	28.8
6	COOCH$_2$	cyclo-hex	9.7	12	CONHCH$_2$	Ph	13.0
7	COO(CH$_2$)$_2$	Ph	4.1	13	CONHCH$_2$	α-napthyl	2.3

[a]The IC_{50}(PfNMT) values were averaged from two independent dose–response curves, the standard deviation was within 30% of the resulting values.

Scheme 2[a]
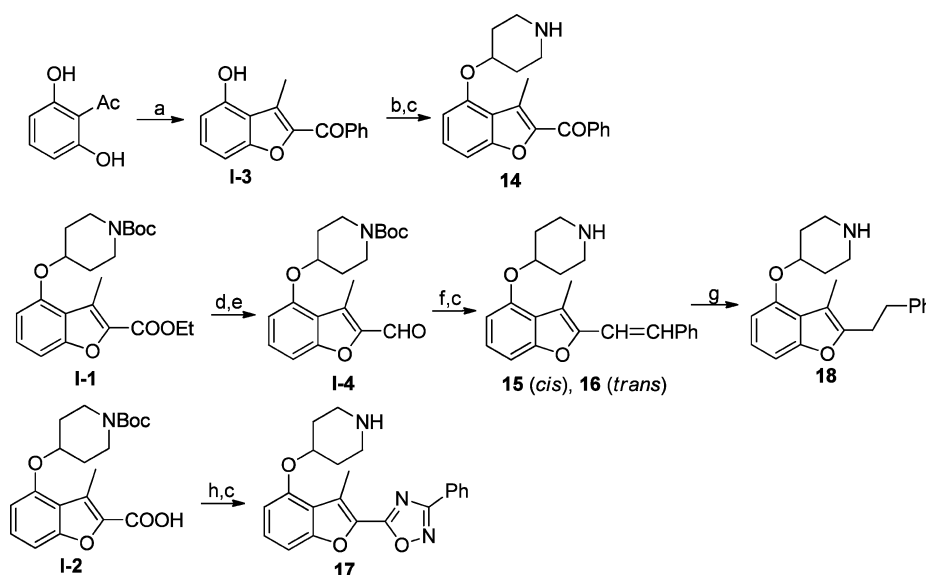
[a]Reagents: (a) PhCOCH$_2$Br, K$_2$CO$_3$, CH$_3$CN, 80 °C, 24 h, 40%; (b) DIAD, PPh$_3$, N-Boc-4-OH piperidine, THF, rt, 4 h, 90%; (c) 5% TFA in DCM, rt, quantitative; (d) LiAlH$_4$, THF, 0 °C to rt, 2 h, 90%; (e) MnO$_2$, DCM, rt, 24 h, 77%; (f) benzyltriphenyl phosphonium bromide, NaOH, THF/H$_2$O, rt, 1 h, 70% (including cis- and trans- isomers); (g) Pd/C, 1,4-cyclohexadiene, EtOH, 80 °C, 4 h, 40%; (f) (i) R^2(NH$_2$)C=N-OH, EDCI, HOBt, DIPEA, CH$_3$CN, rt, 4 h, (ii) 4 Å molecular sieve, dry toluene, 110 °C, 12 h, 70% over two steps.

(4, 5 vs 2, 6 and 12, 13 vs 9, 10), give rise to better enzyme inhibition in both series. Compound 4 represents a significant improvement in potency and has a sub-μM IC_{50} value of 0.27 μM. Introduction of a methylene moiety between R^2 and the ester group was a key factor in this enhanced potency (4 vs 3), suggesting the importance of flexibility in the linker group Y. Furthermore, spacers longer than methylene significantly reduced the affinity (7, 8 vs 4), indicating that this spacing is optimal. Surprisingly, a huge loss of activity was found when the Y linker was altered from a methylene ester to a methylene amide (4 vs 12); however, the deleterious effect of the ester to amide swap is largely mitigated when the phenyl R^2 group is replaced by a napthyl group (5 vs 13), prompting further investigation of the linker group Y to understand its role in binding.

Investigation of Linker Group Y. Compounds containing rigid Y linkers with similar length (14–17) were initially synthesized (Scheme 2). These inhibitors (3, 11, 14–17, Table 2) were found to be only moderately active compared to their

methylene ester analogues, such as 4, reinforcing the earlier conclusion that the flexibility of the Y linker group is crucial. Compounds with various types of flexible Y linkers (18–25, Table 2) were then prepared (Scheme 3). It is clear that a flexible linker alone, such as ethylene 18, does not confer inhibitory activity. Introduction of a heteroatom in the ethylene linker improved enzyme affinity (19, 20 vs 18). Compounds 22–25 were designed to mimic the original methylene ester, with a view to finding a more suitable replacement (Table 2). Both the carbonyl and the ester oxygen atoms in the methylene ester were found to contribute to potency because replacement of either atom by methylene led to a 40-fold activity drop (21, 22 vs 4). Removing a rotatable bond of the ethylene gave a 3-fold improvement in affinity (23 vs 22), which appears to contradict the earlier interpretation that flexibility in the Y linker is important. It is possible that this particular rigid linker directs the pendant phenyl group into a specific hydrophobic cavity. The dramatic loss of activity in 24 is unexpected and cannot be explained by the shorter length of the linker Y

**Table 2. Activities of Inhibitors Containing Different Y Linkers against PfNMT and *P. falciparum*[a]**
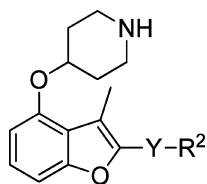
compd no.	Y	R²	IC$_{50}$ (μM)	S. I.[b]	EC$_{50}$ (μM)
3	COO	Ph	24.4	>20	10.0
4	COOCH$_2$	Ph	0.27	>400	1.2
11	CONH	Ph	28.8	>10	5.3
13	CONHCH$_2$	α-napthyl	2.3	28	2.4
14	CO	Ph	22.0	>5	5.3
15	*cis*-CH=CH	Ph	72.0	-	-
16	*trans*-CH=CH	Ph	26.1	>10	n.d.[c]
17		Ph	17.9	>12	n.d.
18	CH$_2$CH$_2$	Ph	131	-	-
19	CH$_2$O	Ph	6.6	>16	n.d.
20[d]	SCH$_2$	Ph	38.2	-	-
21	CH$_2$OCH$_2$	Ph	7.1	14	4.5
22	CO(CH$_2$)$_2$	Ph	10.2	>20	4.0
23		Ph	3.5	14	2.5
24[d]	SO$_2$CH$_2$	Ph	>200	-	-
25		Ph	2.0	>50	2.1
26	COOCH$_2$	3-OMe-Ph	0.60	>200	n.d.

[a]The IC$_{50}$(PfNMT) and EC$_{50}$(*P. falciparum*, 3D7 line) values were averaged from two independent dose−response curves, the standard deviation was within 30% of the resulting values. [b]S.I. = selectivity index, calculated as IC$_{50}$(HsNMT1)/IC$_{50}$(PfNMT). [c]n.d. = not determined. [d]there is no methyl group at the C-3 position of the benzofuran scaffold.

compared to the methylene ester because phenyl ketone **14**, which has an even shorter linker, retains some inhibitory activity with an IC$_{50}$ of 22 μM. Therefore, it is likely that the methylene sulfone is incompatible with the binding site of the enzyme. 1,2,4-oxadiazole **25**, an ester bioisostere, exhibited promising potency and selectivity although it was still less active than its ester counterpart. Given that none of the other Y linkers synthesized showed comparable inhibition, the methylene ester was selected as an optimal linker group (Figure 3). Next, a standard set of substituents (methyl, chloro, and methoxy)

were employed to find suitable substituents on the pendant phenyl ring in the methylene ester series. However, of the seven synthesized compounds, only the *meta*-methoxy substituent in **26** gave comparable potency to the parent compound **4** (Table S4, Supporting Information), indicating a tight R² group binding pocket in the enzyme.

These compounds in Table 2 were also applied to synchronized *P. falciparum* trophozoites (3D7 line). Consistent with the premise that NMT is a good target in *Plasmodium*, it was found that these inhibitors also showed promising

Scheme 3[a]
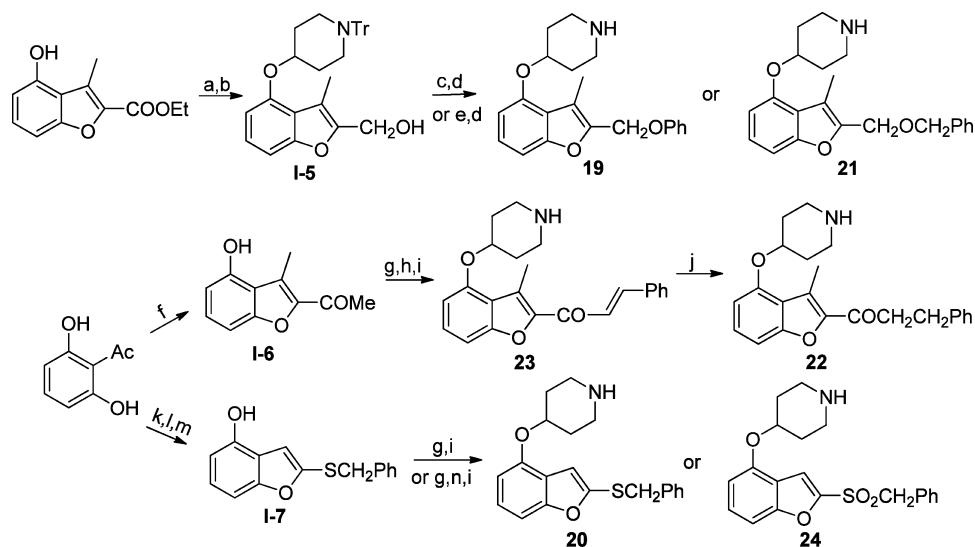
[a]Reagents: (a) DIAD, PPh₃, *N*-Tr-4-OH piperidine, THF, rt, 4 h, 65%; (b) LiAlH₄, THF, 0 °C to rt, 2 h, 90%; (c) DIAD, PPh₃, phenol, THF, rt, 4 h, 5%; (d) 0.1% TFA, 0.2% H₂O in DCM, rt, 90%; (e) NaH, BnBr, DMF, rt, 15%; (f) CH₃COCH₂Cl, K₂CO₃, CH₃CN, 80 °C, 24 h, 20%; (g) DIAD, PPh₃, *N*-Boc-4-OH piperidine, THF, rt, 4 h, 90%; (h) benzaldehyde, NaOH, EtOH/H₂O, 3 h, 45%; (i) 5% TFA in DCM, rt, quantitative; (j) Pd/C, 1,4-cyclohexadiene, EtOH, 80 °C, 4 h, 40%; (k) ethyl carbazate, EtOH/H₂O, 80 °C, 24 h, 24%; (l) SOCl₂, DMF, −20 °C to rt, 3 h, 54%; (m) BnCl, K₂CO₃, dry acetone, 60 °C, 6 h, 24%; (n) *m*-CPBA, DCM, rt, 1 h, 50%.
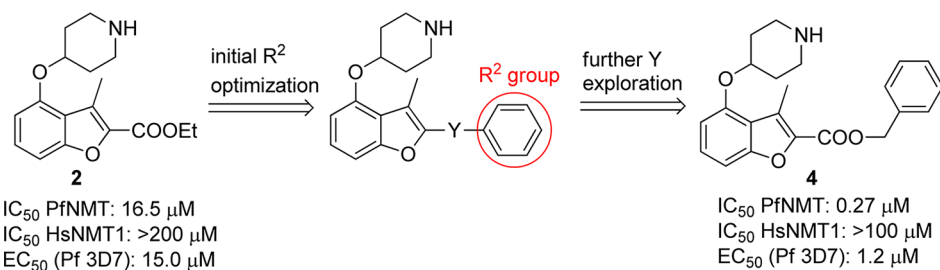

Figure 3. Investigation of *C*-2 side chain.

antiplasmodial effects in vitro, with the most potent PfNMT inhibitor **4** giving the highest antiparasitic activity. These results imply that optimized PfNMT inhibitors have excellent potential to be developed into antimalarial therapeutics.

Structure Studies. Although attempts to crystallize PfNMT have been unsuccessful, we have been able to determine cocrystal structures of *Plasmodium vivax* NMT (PvNMT) with a non-hydrolyzable myr-CoA analogue (NHM)[34] and a series of benzofuran inhibitors. PvNMT shares 81% sequence identity with PfNMT, with only 2 out of 23 residues situated within 5 Å of the ligand differing between the two enzymes (Y212 and Y334 in PvNMT are each replaced by Phe in PfNMT, Figure S1, Supporting Information). Selected compounds from Table 2 were assayed against PvNMT, and similar levels of potency (<3-fold difference) to PfNMT were observed. Therefore, we consider that structures of PvNMT complexes can be used to rationalize the experimental SAR for the PfNMT inhibitors.

Inhibitor **26** occupies what is expected to be the peptide binding pocket of PvNMT (Figure S2, Supporting Information). Its key interactions with the enzyme are illustrated in Figure 4. The secondary amino group of the piperidine establishes an ion pair interaction with the *C*-terminal carboxylate (L410) and a cation−dipole interaction with the phenolic hydroxyl of Y107. The ion pair mimics the interaction of the α-amino groups of substrate peptides with the buried α-carboxylate
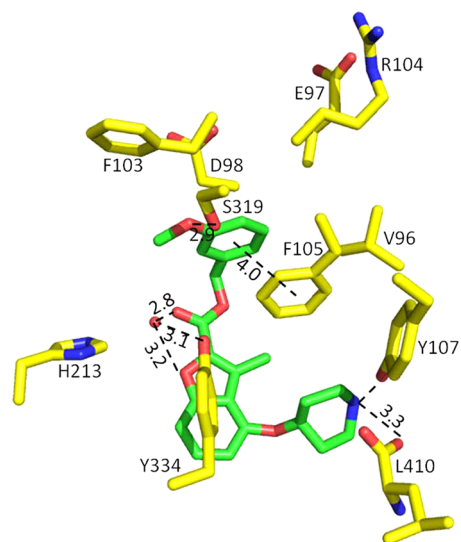

Figure 4. Crystal structure of **26** (1.50 Å resolution, PDB code 4B14) cocrystallized with *P. vivax* NMT. Distances are given in Å. Atoms are colored: C, yellow (enzyme) and green (inhibitor **26**); N, blue; O, red; H₂O, red sphere.

of NMT (as observed in structures of *Saccharomyces cerevisiae* NMT, ScNMT);[35] moreover, similar interactions are formed by
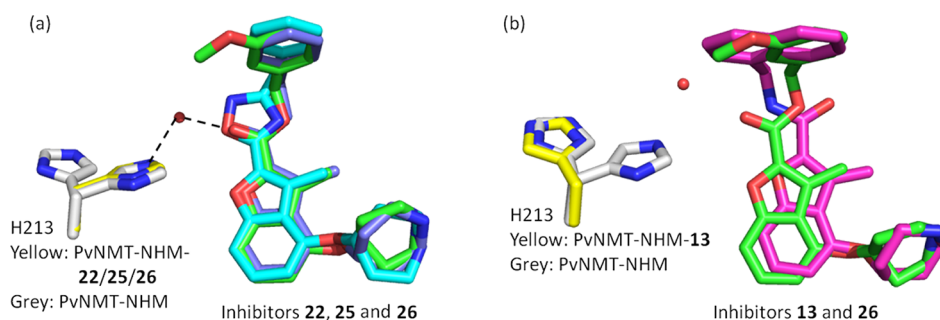
Figure 5. Structural overlays of benzofuran NMT inhibitors: (a) **22** (1.84 Å resolution, PDB code 4B12; C, purple), **25** (1.58 Å resolution, PDB code 4B13; C, cyan), and **26** (PDB code 4B14; C, green) share identical binding positions and rigidify the movement of H213 (binary complex, 1.56 Å resolution, PDB code 4B10; C, gray) to a single conformation (ternary complexes; C, yellow). (b) Opposite orientation adopted by the carbonyl moiety in **13** (1.59 Å resolution, PDB code 4B11; C, magenta) compared to the one in **26** (PDB code 4B14;, C, green) push H213 away from the ligand. Atoms are colored: N, blue; O, red; H_2O, red sphere.

inhibitors of CaNMT[29] and TbNMT.[31] The carbonyl oxygen together with the oxygen atom of the benzofuran ring in **26** participate in water-mediated hydrogen bonds with the hydroxyl of Y334, which may account for the superiority of the methylene ester over its less polar alkyl or ether/thioether equivalents (**18−21** vs **4**). The methylene spacer in **26** allows the pendant aromatic group to be directed into a tight pocket, in agreement with the experimental SAR, where the phenyl group makes π−π interactions with F105 and forms further apolar interactions with residues V96, E97, D98, F103, and R104 that contribute to a loop that closes over the peptide binding pocket. Shorter (**3** vs **4**) or longer (**7**, **8** vs **4**) spacers than the methylene ester result in 10- to 100-fold lower inhibition, presumably because they prevent or compromise the binding of the attached phenyl group to this pocket. Meanwhile the *meta*-methoxy oxygen in **26** forms a hydrogen bond with the hydroxyl of S319.

Inhibitors **22**, **25**, and **26** occupy almost identical binding positions in the enzyme (Figure 5a). Interestingly, binding of these ligands rigidify the side chain of H213, which shows two distinct conformations in the unligated structure but adopts a single conformation that forms water-mediated hydrogen bonds with Y linkers in these compounds (Figure 5a). This indicates an important role for H213 in binding, which is also documented in the binding of a peptide substrate in ScNMT.[36] As seen from the experimental SAR, an amide Y linker is disfavored. The reason for this seemingly surprising result is clarified by examination of the bound structures of these two compounds. It is found that the carbonyl group in **13** adopts the opposite orientation to that of its ester equivalent in **26** (Figure 5b). We believe that this reflects different conformations in the free ligands, presumably due to a steric clash between methyl in the benzofuran scaffold and the hydrogen atom in the amide (Figure 6). Furthermore, the side chain of H213 is observed to move away from the ligand upon the binding of **13** (Figure 5b). This amide carbonyl is hence too far away from either Y334 or H213 to form an interaction and the altered conformation of the spacer might affect the binding geometry of the pendant phenyl ring, which accounts for the large activity difference between amide **12** and ester **4**. However, this difference is largely mitigated when the phenyl R^2 group is replaced by a napthyl group (**13** vs **4**), which makes more extensive π−π interactions with F105.

Selectivity Studies. High inhibitor selectivity between Plasmodial and human NMTs is desirable because NMT is also expressed in human cells. Indeed, our benzofuran inhibitors
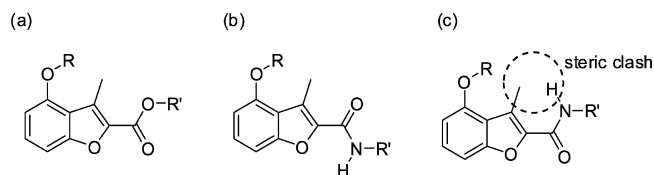

Figure 6. Geometry comparison of ester versus amide inhibitors: (a) Representation of the binding mode of the ester-containing inhibitor **26**. (b) Representation of the binding mode of the amide-containing inhibitor **13**. (c) Alternative conformation of inhibitor **13** does not adopt the conformation found in (a) due to a steric clash between the amide NH and the methyl group.

displayed good to excellent selectivity over HsNMT1 (Table 2). This is surprising in the light of a recent high throughput screening campaign which suggests that strongly selective PfNMT inhibitors would not be easy to identify.[37] The structures were therefore examined with a view to rationalizing the selectivity of the benzofuran compounds.

We compared the structures of PvNMT in its binary complex with NHM and in the ternary complex with NHM and **26**. The side chain of Y211 adopts an alternate conformation upon binding **26** so that there are stacking interactions with the benzofuran ring (Figure 7a). Following superimposition of the structures of PvNMT-NHM−**26** and HsNMT1-Myr-CoA, it is apparent that the equivalent tyrosine (Y296) in the human enzyme occupies a position that would clash with **26** (Figure 7b). Given the weak inhibition of HsNMT1 by **26**, we speculated that a higher energy barrier associated with the conformational change of Y296 in HsNMT1 might be restricting binding. In contrast to **26**, **27** (MRT57965),[38] a PvNMT inhibitor showing little human selectivity, is accommodated in the Plasmodial enzyme with only minor changes in the conformation of Y211 (Figure 7c). It is predicted that similarly small conformational changes of Y296 would be required to accommodate this inhibitor in HsNMT1 (Figure 7d). We therefore hypothesized that steric hindrance by Y296 in HsNMT1 contributes to human selectivity for these benzofuran inhibitors.

To test this hypothesis, site-directed mutagenesis was used to substitute this tyrosine by alanine in both PvNMT and HsNMT1. The inhibitory activities of **25**, **26**, and **27** against the wild-type and mutated NMTs were measured (Table 3) and used to calculate the ratio of the IC_{50} values for HsNMT1 and PvNMT (the selectivity index, SI) for the pair of wild-type enzymes and for the pair of alanine-substituted mutants. The alanine mutations are found to have significantly less selectivity
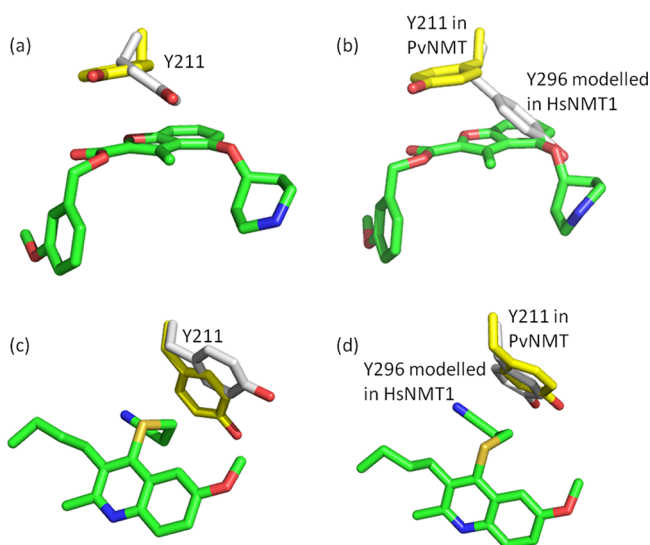
Figure 7. Investigation of selectivity over HsNMT1: (a) Conformational change of Y211 in PvNMT-NHM (PDB code 4B10) upon the binding of **26** (PDB code 4B14). (b) HsNMT1-Myr-CoA (PDB code 3IU1) overlaid with PvNMT-NHM−**26** complex (PDB code 4B14). This indicates a clash between Y296 in HsNMT1 and **26**. (c) Conformational change of Y211 in PvNMT-NHM (PDB code 4B10) upon binding **27**(PDB code 4A95). (d) Overlay of HsNMT1-Myr-CoA (PDB code 3IU1) with PvNMT-NHM−**27** (PDB code 4A95). This suggests minimal conformational changes of that particular tyrosine when binding this inhibitor. Atoms are colored: C, yellow (enzymes in the ternary complex); C, gray (enzymes in the binary complex); C, green (inhibitors); N, blue; O, red; S, gold.

Table 3. The Inhibitory Activity for Mutants of PvNMT and HsNMT1[a]

| inhibitor | IC$_{50}$ (μM) | | | | SI[b] | |
	Pv (WT[c])	Pv (Y211A)	Hs1 (WT)	Hs1 (Y296A)	WT	MU[d]
26	0.6	2.7	45	10	75	3.7
25	6.2	16.6	>500	110	>80	6.6
27[e]	32.7	150	115	218	3.5	1.5

[a]The IC$_{50}$ values were averaged from two independent dose−response curves; the standard deviation was within 30% of the resulting values. [b]SI = selectivity index, calculated by IC$_{50}$(HsNMT1)/IC$_{50}$(PvNMT). [c]WT = wild type. [d]MU = mutants. [e]Wild-type enzyme result for **27** was different from that reported by Goncalves[38] due to different assay conditions, including the concentrations of enzyme, myr-CoA, and different peptide substrate.

for **26** and **25** than the wild-type enzymes, with decreases in the SI of 20-fold and >12-fold, respectively. In contrast, the change in the SI for **27** was only 2-fold. Mutation of the human NMT leads to a 4- to 5-fold increase in affinity for compounds **25** and **26**. This is consistent with the suggestion that changing tyrosine to the smaller alanine in HsNMT1 removes the potential clash and lowers the energy barrier required to accommodate these two inhibitors. On the other hand, under the conditions that only small conformational change is required to accommodate ligand binding (**25**, **26**, and **27** in PvNMT and **27** in HsNMT1), such mutation exclusively led to weaker enzyme affinity, implying that this tyrosine facilitates inhibitor binding to NMTs unless the residue clashes with the bound ligand. The data experimentally demonstrate the contribution of this tyrosine (Y211 in PvNMT and Y296 in HsNMT1) to the human selectivity.

CONCLUSION AND OUTLOOK

Chemistry-driven optimization of a screening hit allowed us to identify PfNMT inhibitor **4** as an early lead candidate with good enzyme and cellular potency and excellent selectivity over human NMT. With the aid of structural information, the superiority of a benzyl ester side chain was rationalized and the interactions involved with the linker were mapped. Furthermore, the structural basis for inhibitory selectivity between HsNMT1 and PfNMT was found to be due to a clash between the inhibitor and residue Y296 in HsNMT1.

Potential biological instability of the ester moiety may limit the scope of inhibitor **4**. Oxadiazole **25**, an ester bioisostere, showed some advantages given its biological stability and comparable cellular potency and human selectivity to **4**; synthesis of oxadiazole analogues shall be the focus of further studies. As suggested by Figure 4, two hotspot residues (F105 and S319 in PvNMT, which are also conserved in PfNMT) are identified to involve a π−π interaction and hydrogen bond with aromatic R^2 respectively. However, as the unsubstituted phenyl ring is still the best R^2 among PfNMT inhibitors so far, it is unlikely that the hydrogen bond with S319 has been formed in PfNMT. Forming this missing hydrogen bond without affecting human selectivity, possibly by using N-containing heterocycles, has the potential to further improve the enzyme potency. Finally, understanding the influence of physiochemical properties (such as pK_a and cLogP) on the cellular potency is also important.

EXPERIMENTAL SECTION

Chemistry. *General Methods.* All solvents and reagents were purchased from commercial sources and used without further purification. The compounds were spotted on silica TLC plates (Merck, Si$_{60}$, F254) and visualized under UV light at 254 nm or iodine over silica. Purification of the compounds for biological tests was performed on a Gilson semipreparative reverse phase HPLC system (Anachem Ltd., Luton, UK) equipped with a HICHROM C$_{18}$ column (250 mm × 21.2 mm), no. 306 pumps, and a Gilson 155 UV/vis detector. UV detection was at 220 nm. The mobile phase consisted of water plus 0.1% TFA (solvent A) and methanol plus 0.1% TFA (solvent B) with a gradient of 30% B for 2 min, changing to 98% B over 30 min, maintaining for 2 min, and then down to 2% B over 0.5 min at a flow rate of 12 mL/min. The purities of the reported compounds for biological assay tests were evaluated by analytical LC-MS which was carried out on a Waters 2767 system equipped with a photodiode array and a mass spectrometer using an X-Bridge C18 column (5 μM, 4.6 mM × 100 mM). The mobile phase consisted of water plus 0.1% formic acid (solvent A) and methanol plus 0.1 formic acid (solvent B) with a gradient starting from 2% to 98% B over the first 10 min, maintaining for 2 min, and down to 2% B over 1 min, followed by the maintenance period for another 4 min at 2% B at a flow rate of 1.2 mL/min. One-dimensional ^{1}H and ^{13}C NMR spectra as well as two-dimensional NMR spectra were recorded on Bruker AV at 400, 500 MHz or 100, 125 MHz, respectively. Chemical shifts are reported in ppm. Mass spectra were obtained from the Mass Spectrometry Service of the Department of Chemistry, Imperial College London. Purity (>95%) and molecular mass of compounds for biological tests were confirmed by LC-MS and high resolution of mass spectrometry.

General Procedure of Mitsunobu Reaction. t-Butyl 4-{[2-(Ethoxycarbonyl)-3-methyl-1-benzofuran-4-yl]oxy}piperidine-1-carboxylate (I-1). To a stirred solution of ethyl 4-hydroxy-3-methylbenzofuran-2-carboxylate[33] (2 g, 9.1 mmol), t-butyl 4-hydrxypiperidine-1-carboxylate (4.56 g, 22.7 mmol) and triphenylphosphine (5.95 g, 22.7 mmol) in anhydrous THF (20 mL) was added DIAD (4.34 mL, 22.7 mmol) dropwise at room temperature. The resulting mixture was stirred at the same temperature for 4 h and then concentrated in vacuo. The residue was purified by column chromatography over silica gel, eluting with hexane:ethyl acetate, 5:1 to afford the title compound as

colorless oil (3.52 g, 96% yield). ^{1}H NMR (CDCl$_3$, 400 MHz): δ 7.32 (t, J = 8.0 Hz, 1H), 7.13 (d, J = 8.0 Hz, 1H), 6.65 (d, J = 8.0 Hz, 1H), 4.74−4.69 (m, 1H), 4.46 (q, J = 7.2 Hz, 2H), 3.68−3.61 (m, 2H), 3.58−3.52 (m, 2H), 2.78 (s, 3H), 2.04−1.97 (m, 2H), 1.96−1.86 (m, 2H), 1.50 (s, 9H), 1.46 (t, J = 7.2 Hz, 3H).

General Procedure for N-Boc Deprotection. Ethyl 3-Methyl-4-(piperidin-4-yloxy)benzofuran-2-carboxylate (2). A mixture of compound **I-1** (10 mg, 0.025 mmol) and TFA (50 μL) in DCM (1 mL) was stirred at room temperature for 2 h. The reaction mixture was evaporated under pressure to dryness, which was further purified by semipreparative reverse phase HPLC to give the title compound as a white solid (9.8 mg, 94% yield). ^{1}H NMR (CD$_3$OD, 400 MHz): δ 7.41 (t, J = 8.4 Hz, 1H), 7.15 (d, J = 8.4 Hz, 1H), 6.88 (d, J = 8.0 Hz, 1H), 4.98−4.93 (m, 1H), 4.42 (q, J = 7.2 Hz, 2H), 3.50−3.40 (m, 2H), 3.33−3.28 (m, 2H), 2.80 (s, 3H), 2.34−2.24 (m, 2H), 2.22−2.12 (m, 2H), 1.43 (t, J = 7.2 Hz, 3H). ^{13}C NMR (CD$_3$OD, 100 MHz): δ 161.87, 157.38, 154.55, 141.09, 130.09, 127.02, 120.30, 106.50, 106.16, 69.95, 62.13, 42.01, 28.28, 14.63, 11.82. Calculated exact mass for the protonated molecule (C$_{17}$H$_{22}$NO$_4$): 304.1549. Measured accurate mass (ESI): 304.1561. LC-MS purity: 100%, R_t = 11.39 min.

Prototypical Procedure for Ester Analogues 3−8 and 26. Phenyl 3-Methyl-4-(piperidin-4-yloxy)-1-benzofuran-2-carboxylate (3). A mixture of compound **I-2** (44 mg, 0.12 mmol), EDCI (25 mg, 0.13 mmol), and hydroxybenzotriazole (22 mg, 0.15 mmol) in anhydrous acetonitrile (3 mL) was stirred at room temperature for 30 min and then treated with phenol (12.1 mg, 0.13 mmol) and DIPEA (41 μL, 0.24 mmol). The resulting mixture was further stirred at room temperature for another 12 h. After that, the solution was evaporated to dryness in vacuo. The residue was redissolved in ethyl acetate (20 mL) and washed with 0.5 M NaOH and brine sequentially. The organic layer was dried over anhydrous sodium sulfate and concentrated in vacuo to produce the *N*-Boc precursor without further purification.

The Boc-deprotection in DCM (2 mL) containing 5% TFA was carried out according to the preparation of compound **2** to afford the title compound as a white solid (28.1 mg, 51% overall yield). ^{1}H NMR (CD$_3$OD, 400 MHz): δ 7.50−7.43 (m, 3H), 7.32 (t, J = 7.6 Hz, 1H), 7.26 (d, J = 7.6 Hz, 2H), 7.18 (d, J = 8.0 Hz, 1H), 6.90 (d, J = 8.0 Hz, 1H), 4.94−4.90 (m, 1H), 3.48−3.41 (m, 2H), 3.35−3.29 (m, 2H), 2.85 (s, 3H), 2.35−2.27 (m, 2H), 2.22−2.14 (m, 2H). ^{13}C NMR (CD$_3$OD, 100 MHz): δ 160.02, 157.66, 154.69, 151.71, 140.26, 130.67, 130.62, 129.16, 127.21, 122.79, 120.29, 106.62, 106.19, 70.09, 41.99, 28.26, 12.05. Calculated exact mass for the protonated molecule (C$_{21}$H$_{22}$NO$_4$): 352.1549. Measured accurate mass (ESI): 352.1545. LC-MS purity: 100%, R_t = 12.17 min.

Prototypical Procedure for Amide Analogues 9−13. N-Isopropyl-3-methyl-4-(piperidin-4-yloxy)benzofuran-2-carboxamide (9). To a solution of compound **I-2** (30 mg, 0.08 mmol) in DMF/DCM (2 mL, 1:1) was sequentially added DIPEA (15 μL, 0.088 mmol) and PyBOP (46 mg, 0.088 mmol). The above mixture was stirred at room temperature for 30 min, followed by the addition of isopropylamine (7.6 μL, 0.088 mmol). The resulting mixture was further stirred at room temperature for 3 h. After that, the reaction mixture was diluted with DCM (15 mL) and partitioned with 0.5 M NaOH solution (15 mL), and then the aqueous layer was further extracted by DCM (10 mL). The combined organic layers were washed brine, dried over anhydrous sodium sulfate, and concentrated in vacuo. The residue was purified by column chromatography over silica gel to afford the *N*-Boc precursor.

The Boc-deprotection in DCM (2 mL) containing 5% TFA was carried out according to the preparation of compound **2** to afford the title compound as a white solid (11.5 mg, 34% overall yield). ^{1}H NMR (CD$_3$OD, 400 MHz): δ 7.37 (t, J = 8.4 Hz, 1H), 7.16 (d, J = 8.4 Hz, 1H), 6.87 (d, J = 8.4 Hz, 1H), 4.98−4.93 (m, 1H), 4.30−4.96 (m, 1H), 3.46−3.40 (m, 2H), 3.32−3.29 (m, 2H), 2.80 (s, 3H), 2.32−2.25 (m, 2H), 2.21−2.13 (m, 2H), 1.29 (d, J = 6.4 Hz, 6H). ^{13}C NMR (CD$_3$OD, 100 MHz): δ 161.52, 156.45, 154.30, 143.11, 129.19, 123.31, 120.78, 106.62, 106.05, 69.78, 42.32, 41.92, 28.23, 22.58, 11.52. Calculated exact mass for the protonated molecule (C$_{18}$H$_{25}$N$_2$O$_3$): 317.1865. Measured accurate mass (ESI): 317.1867. LC-MS purity: 100%, R_t = 10.75 min.

Procedure for Alkenes 15 and 16 and Alkyl 18. 4-({3-Methyl-2-[(Z)-2-phenylethenyl]-1-benzofuran-4-yl}oxy)piperidine (15). The title compound was isolated as second major fraction from the above preparative HPLC (off-white solid, 14.6 mg, 23% overall yield). ^{1}H NMR (CD$_3$OD, 400 MHz): δ 7.58 (d, J = 7.2 Hz, 2H), 7.38 (t, J = 8.0 Hz, 2H), 7.27 (t, J = 7.2 Hz, 1H), 7.23−7.18 (m, 3H), 7.07 (d, J = 8.0 Hz, 1H), 6.78 (d, J = 8.0 Hz, 1H), 4.90−4.82 (m, 1H), 3.46−3.40 (m, 2H), 3.32−3.27 (m, 2H), 2.53 (s, 3H), 2.35−2.22 (m, 2H), 2.21−2.12 (m, 2H). ^{13}C NMR (CD$_3$OD, 100 MHz): δ 157.20, 153.02, 150.95, 138.43, 129.81, 129.62, 128.88, 127.58, 126.80, 121.67, 115.10, 114.66, 106.55, 105.43, 69.62, 41.94, 28.34, 10.52. Calculated exact mass for the protonated molecule (C$_{22}$H$_{24}$NO$_2$): 334.1807. Measured accurate mass (ESI): 334.1799. LC-MS purity: 97%, R_t = 13.64 min.

4-({3-Methyl-2-[(E)-2-phenylethenyl]-1-benzofuran-4-yl}oxy)piperidine (16). To a mixture of compound **I-4** (50 mg, 0.14 mmol) and benzyltriphenyl phosphonium bromide (65 mg, 0.15 mmol) in DCM/water (2 mL, 1:1), 10 M of NaOH solution (50 μL) was added. The resulting mixture was stirred at room temperature for 1 h. After that, the reaction mixture was diluted with DCM (20 mL) and washed sequentially with water and brine (15 mL each). The organic layer was concentrated to give the mixture of the *cis/trans N*-Boc precursors.

The Boc-deprotection in DCM (2 mL) containing 5% TFA was carried out according to the preparation of compound **2** to isolate the title compound as first major fraction from preparative HPLC (white solid, 4.9 mg, 8% overall yield). ^{1}H NMR (CD$_3$OD, 400 MHz): δ 7.41 (d, J = 8.0 Hz, 2H), 7.34−7.26 (m, 3H), 7.17 (t, J = 8.0 Hz, 1H), 6.89 (d, J = 8.0 Hz, 1H), 6.78 (d, J = 8.0 Hz, 1H), 6.72 (d, J = 12.4 Hz, 1H), 6.51 (d, J = 12.4 Hz, 1H), 4.89−4.85 (m, 1H), 3.44−3.37 (m, 2H), 3.31−3.26 (m, 2H), 2.54 (s, 3H), 2.32−2.22 (m, 2H), 2.19−2.11 (m, 2H). ^{13}C NMR (CD$_3$OD, 125 MHz): δ 156.93, 152.96, 150.05, 138.72, 132.03, 130.13, 128.88, 128.52, 127.58, 126.68, 120.99, 116.34, 106.39, 105.56, 69.57, 41.95, 28.32, 11.06. Calculated exact mass for the protonated molecule (C$_{22}$H$_{24}$NO$_2$): 334.1807. Measured accurate mass (ESI): 334.1813. LC-MS purity: 96% (*trans:cis* = 3:1), R_t = 13.22 min.

4-{[3-Methyl-2-(2-phenylethyl)-1-benzofuran-4-yl]oxy}piperidine (18). A mixture of compound **15** (13 mg, 0.039 mmol), palladium on carbon (10% w/w, 5 mg, 0.008 mmol), and 1,4-cyclohexadiene (70 μL) in ethanol (1 mL) was stirred at 80 °C for 4 h. The reaction mixture was then concentrated in vacuo, and the residue was purified by semipreparative reverse phase HPLC to give the title compound as colorless oil (6.6 mg, 38% yield). ^{1}H NMR (CD$_3$OD, 500 MHz): δ 7.23 (t, J = 8.0 Hz, 2H), 7.18−7.11 (m, 4H), 7.03 (d, J = 8.0 Hz, 1H), 6.74 (d, J = 8.0 Hz, 1H), 4.85−4.81 (m, 1H), 3.40−3.35 (m, 2H), 3.30−3.25 (m, 2H), 3.00 (brs, 4H), 2.25−2.19 (m, 2H), 2.15−2.09 (m, 2H), 2.11 (s, 3H). ^{13}C NMR (CD$_3$OD, 125 MHz): δ 157.06, 153.11, 152.38, 142.37, 129.55, 129.31, 127.08, 125.06, 121.20, 111.15, 106.34, 105.55, 69.41, 41.90, 35.44, 29.07, 28.31, 10.17. Calculated exact mass for the protonated molecule (C$_{22}$H$_{26}$NO$_2$): 336.1964. Measured accurate mass (ESI): 336.1964. LC-MS purity: 100%, R_t = 13.30 min.

Procedure for Ethers 19 and 21. 4-{[3-Methyl-2-(phenoxymethyl)-1-benzofuran-4-yl]oxy}piperidine (19). To a stirred solution of compound **I-5** (30 mg, 0.06 mmol), phenol (14.1 mg, 0.15 mmol), and triphenylphosphine (39 mg, 0.15 mmol) in anhydrous THF (2 mL) was added DIAD (29 μL, 0.15 mmol) at room temperature. The resulting mixture was stirred at the same temperature for 4 h and then concentrated in vacuo. The residue was purified by column chromatography over silica gel to afford the *N*-trityl precursor.

The trityl-deprotection was carried out in DCM (1 mL), containing 0.1% of TFA and 0.2% of water, at room temperature for 12 h. After that, the reaction mixture was concentrated in vacuo and the residue was purified by semipreparative reverse phase HPLC, with no TFA in the mobile phases, to afford the title compound as colorless oil (0.4 mg, 2% overall yield). ^{1}H NMR (CD$_3$OD, 400 MHz): δ 7.32−7.28 (m, 2H), 7.24 (t, J = 8.0 Hz, 1H), 7.09 (d, J = 8.0 Hz, 1H), 7.04 (d, J = 8.0 Hz, 2H), 6.98 (t, J = 8.0 Hz, 1H), 6.81 (d, J = 8.0 Hz, 1H), 5.15 (s, 2H), 4.96−4.89 (m, 1H), 3.43−3.38 (m, 2H), 3.30−3.26 (m, 2H), 2.48 (s, 3H), 2.30−2.22 (m, 2H), 2.20−2.11 (m, 2H). ^{13}C NMR (CD$_3$OD, 125 MHz): δ 159.96, 153.18, 148.70, 138.03,

130.54, 126.75, 122.40, 120.63, 116.18, 115.81, 106.33, 105.89, 69.55, 61.90, 41.98, 28.34, 10.50. Calculated exact mass for the protonated molecule ($C_{21}H_{24}NO_3$): 338.1756. Measured accurate mass (ESI): 338.1772. LC-MS purity: 100%, R_t = 12.44 min.

4-({2-[(Benzyloxy)methyl]-3-methyl-1-benzofuran-4-yl}oxy)-piperidine (21). A solution of **I-4** (30 mg, 0.06 mmol) and sodium hydride (60% w/w, 7.2 mg, 0.18 mmol) in anhydrous DMF was stirred at room temperature for 30 min and then treated with benzyl bromide (10.7 μL, 0.09 mmol). The resulting mixture was further stirred at room temperature for 12 h. After that, the reaction mixture was quenched with 100 μL of cold water, diluted with EtOAc (20 mL), and sequentially washed with water and brine (each for 20 min). The organic layer was concentrated in vacuo, and the residue was purified by column chromatography over silica gel to give the *N*-trityl precursor.

The trityl-deprotection was carried out in DCM (1 mL), containing 0.1% of TFA and 0.2% of water, at room temperature for 12 h. After that, the reaction mixture was concentrated in vacuo and the residue was purified by semipreparative reverse phase HPLC, with no TFA in the mobile phases, to afford the title compound as colorless oil (2 mg, 10% overall yield). ¹H NMR (CD₃OD, 400 MHz): δ 7.40−7.28 (m, 5H), 7.23 (t, *J* = 8.0 Hz, 1H), 7.09 (d, *J* = 8.0 Hz, 1H), 6.81 (d, *J* = 8.0 Hz, 1H), 4.91−4.85 (m, 1H), 4.64 (s, 2H), 4.60 (s, 2H), 3.46−3.39 (m, 2H), 3.30−3.27 (m, 2H), 2.43 (s, 3H), 2.30−2.22 (m, 2H), 2.20−2.12 (m, 2H). ¹³C NMR (CD₃OD, 125 MHz): δ 156.06, 151.72, 148.30, 137.87, 128.02, 127.62, 127.45, 125.19, 119.22, 114.14, 104.84, 104.45, 71.65, 68.06, 61.44, 40.53, 26.90, 9.14. Calculated exact mass for the protonated molecule ($C_{22}H_{26}NO_3$): 352.1913. Measured accurate mass (ESI): 352.1909. LC-MS purity: 100%, R_t = 12.34 min.

(2E)-1-[3-Methyl-4-(piperidin-4-yloxy)-1-benzofuran-2-yl]-3-phenylprop-2-en-1-one (23). Prepared from a solution of compound **I-6** (190 mg, 1.0 mmol), *t*-butyl 4-hydrxypiperidine-1-carboxylate (500 mg, 2.5 mmol), triphenylphosphine (657 mg, 2.5 mmol), and DIAD (480 μL, 2.5 mmol) in anhydrous THF (4 mL) according to the procedure of making compound **I-1**. *t*-Butyl 4-[(2-acetyl-3-methyl-1-benzofuran-4-yl)oxy]piperidine-1-carboxylate was obtained as a light-yellow solid (318 mg).

Above solid (50 mg, 0.13 mmol) and benzaldehyde (15 μL, 0.15 mmol) in ethanol (1 mL) was added 0.25 M NaOH solution (1 mL). The mixture was stirred at room temperature for 3 h and then diluted with 20 mL of EtOAc, followed by the wash with water and brine (20 mL each). The organic layer was dried over anhydrous sodium sulfate and concentrated in vacuo. The residue was purified by column chromatography over silica gel to give the *N*-Boc precursor.

The *N*-Boc deprotection was carried out in DCM containing 5% TFA (2 mL) according to the preparation of compound **2** to afford the title compound as a yellow solid (14.7 mg, 24% overall yield). ¹H NMR (CD₃OD, 400 MHz): δ 7.86−7.75 (m, 4H), 7.51−7.45 (m, 4H), 7.24 (d, *J* = 8.0 Hz, 1H), 6.89 (d, *J* = 8.0 Hz, 1H), 5.02−4.93 (m, 1H), 3.50−3.39 (m, 2H), 3.33−3.27 (m, 2H), 2.88 (s, 3H), 2.36−2.24 (m, 2H), 2.24−2.12 (m, 2H). ¹³C NMR (CD₃OD, 100 MHz): δ 183.19, 157.14, 154.95, 148.89, 145.04, 136.18, 131.91, 130.81, 130.14, 129.73, 127.50, 123.26, 120.94, 106.64, 106.38, 70.04, 41.99, 28.26, 12.17. Calculated exact mass for the protonated molecule ($C_{23}H_{24}NO_3$): 362.1756. Measured accurate mass (ESI): 362.1750. LC-MS purity: 97%, R_t = 13.17 min.

4-{[2-(Phenylmethane)sulfonyl-1-benzofuran-4-yl]oxy}piperidine (24). A mixture of *t*-butyl 4-{[2-(benzylsulfanyl)-1-benzofuran-4-yl]oxy} piperidine-1-carboxylate (20 mg, 0.046 mmol) and 3-chloroperbenzoic acid (77% w/w, 16 mg, 0.07 mmol) in DCM (1 mL) was stirred at room temperature for 1 h. The reaction mixture was concentrated in vacuo to give the *N*-Boc precursor without further purification.

The *N*-Boc deprotection was carried out in DCM containing 5% TFA (2 mL) according to the preparation of compound **2** to afford the title compound as pink oil (8.0 mg, 36% overall yield). ¹H NMR (CD₃OD, 400 MHz): δ 7.52 (t, *J* = 8.0 Hz, 1H), 7.46 (s, 1H), 7.35−7.21 (m, 6H), 6.99 (d, *J* = 8.0 Hz, 1H), 4.98−4.92 (m, 1H), 4.72 (s, 2H), 3.48−3.39 (m, 2H), 3.29−3.19 (m, 2H), 2.28−2.18 (m, 2H), 2.14−2.07 (m, 2H). ¹³C NMR (CD₃OD, 100 MHz): δ 157.59, 151.61,

148.00, 130.60, 129.39, 128.55, 128.22, 127.77, 117.35, 112.47, 106.75, 105.11, 68.95, 60.60, 40.31, 26.78. Calculated exact mass for the protonated molecule ($C_{20}H_{22}NO_4S$): 372.1270. Measured accurate mass (ESI): 372.1263. LC-MS purity: 100%, R_t = 10.91 min.

Biology. *Enzyme Inhibition Assay.* Measurement of the ability of compounds to inhibit NMTs was performed in 96-well plates using a modification of the scintillation proximity assay platform:[39] each well (in total 100 μL) contained variable amounts of an inhibitor, 9.4 ng of purified PfNMT (4.8 ng for PvNMT, 19.2 ng for PvNMT^Y211A, 5.1 ng for HsNMT1, and 20.4 ng for HsNMT1^Y296A), 62.5 nM ³H-myristoyl-CoA (8 Ci/mmol, purchased from Perkin-Elmer), and 500 nM of the peptide substrate (GLYVSRLFNRLFQKK(Biotin)-NH₂) in 4% DMSO buffer (30 mM Tris, pH 7.4, 0.5 mM EGTA, 0.5 mM EDTA, 2.5 mM DTT, 0.1% Triton X-100). Incubation was allowed to proceed for 30 min at 37 °C, followed by the addition of 100 μL of 1 mg/mL streptavidin PVT beads (purchased from Perkin-Elmer) in a stop solution (200 mM phosphoric acid/NaOH, pH 4, 750 mM MgCl₂, 0.05% (w/V) BSA, 0.01% (w/V) NaN₃) to terminate the reaction. Overnight settling of the beads resulted in an accurate reading, with signal-to-noise ratio at least 20. The instrument used for counting is a Plate Chameleon multilabel reader (Hidex Oy, Finland). The readout of [³H]-myristoylated peptide in the reaction lacking an inhibitor was defined as 100% activity (positive control) and that from the reaction with no enzyme was defined as 0% (negative control). The effect of an inhibitor at the single concentration was calculated as a percentage of the enzyme activity left (% activity left = (readout-negative)/(positive-negative) × 100%). In terms of the IC₅₀ determination, the inhibitory activity of an inhibitor was measured according to the method described above with the concentrations ranging from 500 μM to 2 nM and the 50% inhibitory concentration (IC₅₀) of an inhibitor was calculated by a nonlinear regression analysis using GraFit 7.0.1 version (Erithacus Software Limited, UK). The assays were carried out in duplicate.

P. falciparum Inhibition Assay. Measurement of the ability of compounds to kill parasites was performed in 96-well plates using a modification of the fluorescent-activity cell sorting (FACS) assay platform:[40,41] each well (in total 100 μL, 0.5% DMSO) contained synchronous cultures of late trophozoite-stage parasites (1% parasitemia and 2% hematocrit) and variable concentrations of an inhibitor. The mixture was incubated at 37 °C for a full 48 h growth cycle. Aliquots of 50 μL were removed from each well, added to 500 μL of freshly diluted hydroethidine (HE, 1:200 dilution of 10 mg/mL DMSO stock in PBS), and incubated for 20 min at 37 °C. Samples were then diluted with 1 mL of PBS to enable appropriate cell counts (50000) and stored on ice. Parasites cultured in the absence of an inhibitor, and noninfected red blood cells were used as positive and negative controls, respectively. Parasitemia was measured using a FACS Calibur flow cytometer. Growth inhibition at each concentration was calculated as % inhibition = [1 − (readout-negative control)/(positive-negative control)] × 100%. To determine the EC₅₀ of an inhibitor, its activity at a range of concentrations from 10 μM down to 0.31 μM and the 50% inhibitory concentration (EC₅₀) of an inhibitor was calculated by a nonlinear regression analysis using GraFit 7.0.1 version (Erithacus Software Limited, UK). All assays were carried out in triplicate.

Crystallography. *Protein Expression, Purification, and Crystallization.* For HsNMT1, a clone directing the synthesis of a protein without the first 108 amino acid residues corresponding to the NMT catalytic domain was expressed in *Escherichia coli* and purified as described in reference.[34] PvNMT expression and purification followed protocols as described in ref 38 . Mutagenesis of PvNMT Y211 and HsNMT Y296 residues to alanine was performed using a QuikChange Lightning site-directed mutagenesis kit (Stratagene). Initial crystals of a binary complex with a nonhydrolyzable cofactor (PvNMT-NHM) were grown from a solution of protein (6 mg/mL) containing 1/20th volume of *S*-(2-oxo) pentadecyl-coenzyme A (NHM, 10 mM in 50% DMSO) and an equal volume of IndexScreen (Hampton) solution F7 (0.2 M ammonium sulfate and 25% (w/v) PEG 3350 in 0.1 M Bis-Tris buffer, pH 6.5). The crystals belong to the orthorhombic space group $P2_12_12_1$.The structure was solved by molecular replacement in the

program MOLREP[42] using the protein coordinates of NMT from *Leishmania donovani* (PDB code 2WUU)[43] as the search model. Three solutions (a trimer) were found, corresponding to a Matthew's coefficient of 2.22 Å³/Da and a solvent content of 44.5%, and this trimer was used as the basis for structure determination of ternary complexes of PvNMT-NHM containing ligands (Table S5, Supporting Information). For crystallization of the ligand complexes, PvNMT was incubated overnight at 4 °C, with NHM as above plus solid ligand (compounds **25** and **26**) or 1/20th volume ligand (compounds **13** and **22**, 10 mM in 50% DMSO). Crystals were grown by the vapor diffusion method, typically from sitting drops consisting of 0.3 μL of protein mixture (after centrifugation to pellet any solid material) and 0.3 μL of reservoir solution containing 0.2 M ammonium sulfate, 24–26% (w/v) PEG 3350, in 0.1 M Bis-Tris or MES buffer, pH 6.0–6.5, equilibrated against 0.1 mL of reservoir solution in 48-well plates at 20 °C. Crystals were vitrified directly in liquid nitrogen before storage.

Data Collection, Processing, and Refinement. X-ray diffraction data were collected on synchrotron beamlines at the Diamond Light Source (DLS), Oxford, and processed using XDS[44] and SCALA[45] implemented within *xia2*.[46] Data collection and refinement statistics are summarized in Supporting Information Table S5. For R_{free} calculations, 5% of the data were excluded and the R_{free} flags for each ternary complex structure solution were copied from the binary complex structure (PvNMT-NHM). Rigid Body refinement using maximum likelihood methods implemented in REFMAC[47] was followed by a cycle of model building and adjustment using COOT[48] and five cycles of refinement using anisotropic temperature factors. Electron density maps from this early stage of refinement calculated using phases unbiased by contributions from ligand ("omit" maps) are presented in Figure S3, Supporting Information. Complete chains (corresponding to residues 26–410, numbering as in full-length protein) can be traced for two of the three molecules in the asymmetric unit. N-Terminal residues (remaining from the tag) in all three chains and loop residues 227–238 in chain C have not been modeled, and these are assumed to be disordered. The protein structure models display good geometry with 95.9% of the residues in the preferred region of the Ramachandran plot, with an additional 3.9% in allowed regions and 0.2% (corresponding to two residues in chain C) as outliers. For ligand cocrystal structures, three residues (F336 in all three chains) also appear in outlying regions of the plot.

ASSOCIATED CONTENT

ⓢ Supporting Information

Synthetic details for all compounds, additional compound biological data, alignment of PvNMT and PfNMT, and X-ray crystallographic data. This material is available free of charge via the Internet at http://pubs.acs.org.

Accession Codes

The coordinates and structure factor files have been deposited in the Protein Data Bank under the accession codes 4B10 (PvNMT-NHM), 4B11 (PvNMT-NHM–**13**), 4B12 (PvNMT-NHM–**22**), 4B13 (PvNMT-NHM–**25**), and 4B14 (PvNMT-NHM–**26**).

AUTHOR INFORMATION

Corresponding Author

*For E.W.T.: phone, +44 2075 943 752; E-mail, e.tate@imperial.ac.uk. For R.J.L.: phone, +44 2075 945 752; E-mail, r.leatherbarrow@imperial.ac.uk.

Notes

The authors declare no competing financial interest.

ACKNOWLEDGMENTS

ABBREVIATION USED

NMT, *N*-myristoyltransferase; myr-CoA, myristoyl-coenzyme A; NHM, nonhydrolyzable myristoyl-coenzyme A; SAR, structure–activity relationship; PDB, Protein Data Bank; Ph, phenyl; *i*-Pr, *iso*-propyl; Et, ethyl; hex, hexane; Boc, *tert*-butoxycarbonyl; Tr, trityl

REFERENCES

(1) *World Malaria Report 2011*; World Health Organization: Geneva, 2011.

(2) Opar, A. Quarter-century quest for malaria vaccine shows signs of success. *Nature Rev. Drug Discovery* **2011**, *10*, 887–888.

(3) Hyde, J. E. Drug-resistant malaria—an insight. *FEBS J.* **2007**, *274*, 4688–4698.

(4) *Guidelines for the Treatment of Malaria*, 2nd ed.; World Health Organization: Geneva, 2010; pp 13–47.

(5) Dondorp, A. M.; Nosten, F.; Yi, P.; Das, D. Artemisinin resistance in *Plasmodium falciparum* malaria. *N. Engl. J. Med.* **2009**, *361*, 455–467.

(6) Gamo, F.-J.; Sanz, L. M.; Vidal, J.; de Cozar, C.; Alvarez, E.; Lavandera, J.-L.; Vanderwall, D. E.; Green, D. V. S.; Kumar, V.; Hasan, S.; Brown, J. R.; Peishoff, C. E.; Cardon, L. R.; Garcia-Bustos, J. F. Thousands of chemical starting points for antimalarial lead identification. *Nature* **2010**, *465*, 305–310.

(7) Plouffe, D.; Brinker, A.; McNamara, C.; Henson, K.; Kato, N.; Kuhen, K.; Nagle, A.; Adrian, F.; Matzen, J. T.; Anderson, P.; Nam, T.-g.; Gray, N. S.; Chatterjee, A.; Janes, J.; Yan, S. F.; Trager, R.; Caldwell, J. S.; Schultz, P. G.; Zhou, Y.; Winzeler, E. A. In silico activity profiling reveals the mechanism of action of antimalarials discovered in a high-throughput screen. *Proc. Natl. Acad. Sci. U.S.A.* **2008**, *105*, 9059–9064.

(8) Rottmann, M.; McNamara, C.; Yeung, B. K. S.; Lee, M. C. S.; Zou, B.; Russell, B.; Seitz, P.; Plouffe, D. M.; Dharia, N. V.; Tan, J.; Cohen, S. B.; Spencer, K. R.; Gonzalez-Paez, G. E.; Lakshminarayana, S. B.; Goh, A.; Suwanarusk, R.; Jegla, T.; Schmitt, E. K.; Beck, H.-P.; Brun, R.; Nosten, F.; Renia, L.; Dartois, V.; Keller, T. H.; Fidock, D. A.; Winzeler, E. A.; Diagana, T. T. Spiroindolones, A Potent Compound Class for the Treatment of Malaria. *Science* **2010**, *329*, 1175–1180.

(9) O'Neill, P. M.; Amewu, R. K.; Nixon, G. L.; Bousejra ElGarah, F.; Mungthin, M.; Chadwick, J.; Shone, A. E.; Vivas, L.; Lander, H.; Barton, V.; Muangnoicharoen, S.; Bray, P. G.; Davies, J.; Park, B. K.; Wittlin, S.; Brun, R.; Preschel, M.; Zhang, K.; Ward, S. A. Identification of a 1,2,4,5-Tetraoxane Antimalarial Drug-Development Candidate (RKA 182) with Superior Properties to the Semisynthetic Artemisinins. *Angew. Chem., Int. Ed.* **2010**, *49*, 5693–5697.

(10) Meister, S.; Plouffe, D. M.; Kuhen, K. L.; Bonamy, G. M. C.; Wu, T.; Barnes, S. W.; Bopp, S. E.; Borboa, R.; Bright, A. T.; Che, J.; Cohen, S.; Dharia, N. V.; Gagaring, K.; Gettayacamin, M.; Gordon, P.; Groessl, T.; Kato, N.; Lee, M. C. S.; McNamara, C. W.; Fidock, D. A.; Nagle, A.; Nam, T.-g.; Richmond, W.; Roland, J.; Rottmann, M.; Zhou, B.; Froissard, P.; Glynne, R. J.; Mazier, D.; Sattabongkot, J.; Schultz, P. G.; Tuntland, T.; Walker, J. R.; Zhou, Y.; Chatterjee, A.; Diagana, T. T.; Winzeler, E. A. Imaging of Plasmodium Liver Stages to Drive Next-Generation Antimalarial Drug Discovery. *Science* **2011**, *334*, 1372–1377.

(11) Bowyer, P. W.; Tate, E. W.; Leatherbarrow, R. J.; Holder, A. A.; Smith, D. F.; Brown, K. A. *N*-Myristoyltransferase: A Prospective Drug Target for Protozoan Parasites. *ChemMedChem* **2008**, *3*, 402–408.

(12) Duronio, R. J.; Towler, D. A.; Heuckeroth, R. O.; Gordon, J. I. Disruption of the yeast *N*-myristoyl transferase gene causes recessive lethality. *Science* **1989**, *243*, 796–800.

(13) Lodge, J. K.; Jackson-Machelski, E.; Toffaletti, D. L.; Perfect, J. R.; Gordon, J. I. Targeted gene replacement demonstrates that myristoyl-CoA: protein N-myristoyltransferase is essential for viability of *Cryptococcus neoformans*. *Proc. Natl. Acad. Sci. U.S.A.* **1994**, *91*, 12008–12012.

(14) Weinberg, R. A.; McWherter, C. A.; Freeman, S. K.; Wood, D. C.; Gordon, J. I.; Lee, S. C. Genetic studies reveal that myristoylCoA:protein N-myristoyltransferase is an essential enzyme in *Candida albicans*. *Mol. Microbiol.* **1995**, *16*, 241–250.

(15) Price, H. P.; Menon, M. R.; Panethymitaki, C.; Goulding, D.; McKean, P. G.; Smith, D. F. Myristoyl-CoA:Protein N-Myristoyltransferase, An Essential Enzyme and Potential Drug Target in Kinetoplastid Parasites. *J. Biol. Chem.* **2003**, *278*, 7206–7214.

(16) Johnson, D. R.; Bhatnagar, R. S.; Knoll, L. J.; Gordon, J. I. Genetic and Biochemical Studies of Protein N-Myristoylation. *Annu. Rev. Biochem.* **1994**, *63*, 869–914.

(17) Wright, M.; Heal, W.; Mann, D.; Tate, E. Protein myristoylation in health and disease. *J. Chem. Biol.* **2010**, *3*, 19–35.

(18) Rees-Channer, R. R.; Martin, S. R.; Green, J. L.; Bowyer, P. W.; Grainger, M.; Molloy, J. E.; Holder, A. A. Dual acylation of the 45 kDa gliding-associated protein (GAP45) in *Plasmodium falciparum* merozoites. *Mol. Biochem. Parasitol.* **2006**, *149*, 113–116.

(19) Stafford, W. H. L.; Stockley, R. W.; Ludbrook, S. B.; Holder, A. A. Isolation, Expression and Characterization of the Gene for an ADP-Ribosylation Factor from the Human Malaria Parasite, Plasmodium Falciparum. *Eur. J. Biochem.* **1996**, *242*, 104–113.

(20) Leber, W.; Skippen, A.; Fivelman, Q. L.; Bowyer, P. W.; Cockcroft, S.; Baker, D. A. A unique phosphatidylinositol 4-phosphate 5-kinase is activated by ADP-ribosylation factor in *Plasmodium falciparum*. *Int. J. Parasitol.* **2009**, *39*, 645–653.

(21) Green, J. L.; Rees-Channer, R. R.; Howell, S. A.; Martin, S. R.; Knuepfer, E.; Taylor, H. M.; Grainger, M.; Holder, A. A. The Motor Complex of *Plasmodium falciparum*. *J. Biol. Chem.* **2008**, *283*, 30980–30989.

(22) Pino, P.; Graindorge, A.; Kim, A.; Soldati-Favre, D. Conditional system for the malaria parasites: functional dissection of N-myristoyltransferase and rhomboid 4 genes in *Plasmodium berghei*. Molecular Approaches to Malaria 2012, Lorne, Australia, February 19–23, 2012.

(23) Rudnick, D. A.; McWherter, C. A.; Rocque, W. J.; Lennon, P. J.; Getman, D. P.; Gordon, J. I. Kinetic and structural evidence for a sequential ordered Bi–Bi mechanism of catalysis by *Saccharomyces cerevisiae* myristoyl-CoA:protein N-myristoyltransferase. *J. Biol. Chem.* **1991**, *266*, 9732–9739.

(24) Masubuchi, M.; Ebiike, H.; Kawasaki, K.; Sogabe, S.; Morikami, K.; Shiratori, Y.; Tsujii, S.; Fujii, T.; Sakata, K.; Hayase, M.; Shindoh, H.; Aoki, Y.; Ohtsuka, T.; Shimma, N. Synthesis and biological activities of benzofuran antifungal agents targeting fungal N-myristoyltransferase. *Bioorg. Med. Chem.* **2003**, *11*, 4463–4478.

(25) Kawasaki, K.; Masubuchi, M.; Morikami, K.; Sogabe, S.; Aoyama, T.; Ebiike, H.; Niizuma, S.; Hayase, M.; Fujii, T.; Sakata, K.; Shindoh, H.; Shiratori, Y.; Aoki, Y.; Ohtsuka, T.; Shimma, N. Design and synthesis of novel benzofurans as a new class of antifungal agents targeting fungal N-myristoyltransferase. Part 3. *Bioorg. Med. Chem. Lett.* **2003**, *13*, 87–91.

(26) Ebiike, H.; Masubuchi, M.; Liu, P. L.; Kawasaki, K.; Morikami, K.; Sogabe, S.; Hayase, M.; Fujii, T.; Sakata, K.; Shindoh, H.; Shiratori, Y.; Aoki, Y.; Ohtsuka, T.; Shimma, N. Design and synthesis of novel benzofurans as a new class of antifungal agents targeting fungal N-myristoyltransferase. Part 2. *Bioorg. Med. Chem. Lett.* **2002**, *12*, 607–610.

(27) Yamazaki, K.; Kaneko, Y.; Suwa, K.; Ebara, S.; Nakazawa, K.; Yasuno, K. Synthesis of potent and selective inhibitors of *Candida albicans* N-myristoyltransferase based on the benzothiazole structure. *Bioorg. Med. Chem.* **2005**, *13*, 2509–2522.

(28) Devadas, B.; Freeman, S. K.; Zupec, M. E.; Lu, H. F.; Nagahashi, S.; Kishore, N. S.; Lodge, J. K.; Kuneman, D. W.; McWherter, C. A.; Vinjamoori, D. V.; Getman, D. P.; Gordon, J. I.; Sikorski, J. A. Design and synthesis of novel imidazole-substituted dipeptide amides as potent and selective inhibitors of *Candida albicans* myristoyl-CoA:protein N-myristoyltransferase and identification of related tripeptide inhibitors with mechanism-based antifungal activity. *J. Med. Chem.* **1997**, *40*, 2609–2625.

(29) Masubuchi, M.; Kawasaki, K.; Ebiike, H.; Ikeda, Y.; Tsujii, S.; Sogabe, S.; Fujii, T.; Sakata, K.; Shiratori, Y.; Aoki, Y.; Ohtsuka, T.; Shimma, N. Design and synthesis of novel benzofurans as a new class of antifungal agents targeting fungal N-myristoyltransferase. Part 1. *Bioorg. Med. Chem. Lett.* **2001**, *11*, 1833–1837.

(30) Gelb, M. H.; Van Voorhis, W. C.; Buckner, F. S.; Yokoyama, K.; Eastman, R.; Carpenter, E. P.; Panethymitaki, C.; Brown, K. A.; Smith, D. F. Protein farnesyl and N-myristoyl transferases: piggy-back medicinal chemistry targets for the development of antitrypanosomatid and antimalarial therapeutics. *Mol. Biochem. Parasitol.* **2003**, *126*, 155–163.

(31) Brand, S.; Cleghorn, L. A. T.; McElroy, S. P.; Robinson, D. A.; Smith, V. C.; Hallyburton, I.; Harrison, J. R.; Norcross, N. R.; Spinks, D.; Bayliss, T.; Norval, S.; Stojanovski, L.; Torrie, L. S.; Frearson, J. A.; Brenk, R.; Fairlamb, A. H.; Ferguson, M. A. J.; Read, K. D.; Wyatt, P. G.; Gilbert, I. H. Discovery of a Novel Class of Orally Active Trypanocidal N-Myristoyltransferase Inhibitors. *J. Med. Chem.* **2012**, *55*, 140–152.

(32) Frearson, J. A.; Brand, S.; McElroy, S. P.; Cleghorn, L. A. T.; Smid, O.; Stojanovski, L.; Price, H. P.; Guther, M. L. S.; Torrie, L. S.; Robinson, D. A.; Hallyburton, I.; Mpamhanga, C. P.; Brannigan, J. A.; Wilkinson, A. J.; Hodgkinson, M.; Hui, R.; Qiu, W.; Raimi, O. G.; van Aalten, D. M. F.; Brenk, R.; Gilbert, I. H.; Read, K. D.; Fairlamb, A. H.; Ferguson, M. A. J.; Smith, D. F.; Wyatt, P. G. N-Myristoyltransferase inhibitors as new leads to treat sleeping sickness. *Nature* **2010**, *464*, 728–732.

(33) Belanger, P. C.; Dufresne, C.; Lau, C. K.; Scheigetz, J. An improved synthesis of ethyl 4-hydroxy-3-methylbenzofuran-2-carboxylate. *Org. Prep. Proced. Int.* **1988**, *20*, 299–302.

(34) Goncalves, V.; Brannigan, J. A.; Thinon, E.; Olaleye, T. O.; Serwa, R.; Lanzarone, S.; Wilkinson, A. J.; Tate, E. W.; Leatherbarrow, R. J. A fluorescence-based assay for N-myristoyltransferase activity. *Anal. Biochem.* **2012**, *421*, 342–344.

(35) Farazi, T. A.; Manchester, J. K.; Waksman, G.; Gordon, J. I. Pre-Steady-State Kinetic Studies of *Saccharomyces cerevisiae* Myristoyl-CoA:Protein N-Myristoyltransferase Mutants Identify Residues Involved in Catalysis. *Biochemistry* **2001**, *40*, 9177–9186.

(36) Wu, J. T. Y.; Zhang, M. L.; Howard, M. H.; Gutteridge, S.; Ding, J. P. Crystal Structures of *Saccharomyces cerevisiae* N-Myristoyltransferase with Bound Myristoyl-CoA and Inhibitors Reveal the Functional Roles of the N-terminal Region. *J. Biol. Chem.* **2007**, *282*, 22185–22194.

(37) Bell, A. S.; Mills, J. E.; Williams, G. P.; Brannigan, J. A.; Wilkinson, A. J.; Parkinson, T.; Leatherbarrow, R. J.; Tate, E. W.; Holder, A. A.; Smith, D. F. Selective Inhibitors of Protozoan Protein N-myristoyltransferases as Starting Points for Tropical Disease Medicinal Chemistry Programs. *PLoS Negl. Trop. Dis.* **2012**, *6*, e1625.

(38) Goncalves, V.; Brannigan, J. A.; Whalley, D.; Ansell, K. H.; Saxty, B.; Holder, A. A.; Wilkinson, A. J.; Tate, E. W.; Leatherbarrow, R. J. Discovery of *Plasmodium vivax* N-Myristoyltransferase Inhibitors: Screening, Synthesis, and Structural Characterization of their Binding Mode. *J. Med. Chem.* **2012**, *55*, 3578–3582.

(39) Panethymitaki, C.; Bowyer, P. W.; Price, H. P.; Leatherbarrow, R. J.; Brown, K. A.; Smith, D. F. Characterization and selective inhibition of myristoyl-CoA:protein N-myristoyltransferase from *Trypanosoma brucei* and *Leishmania major*. *Biochem. J.* **2006**, *396*, 277–285.

(40) Bergmann-Leitner, E. S.; Dundcan, E. H.; Mullen, G. E.; Burge, J. R.; Khan, F.; Long, C. A.; Angov, E.; Lyon, J. A. Critical evaluation of different methods for measuring the functional activity of antibodies against malaria bolld stage antigens. *Am. J. Trop. Med. Hyg.* **2006**, *75*, 437–442.

(41) Moss, D. K.; Remarque, E. J.; Faber, B. W.; Cavanagh, D. R.; Arnot, D. E.; Thomas, A. W.; Holder, A. A. *Plasmodium falciparum* 19-Kilodalton Merozoite Surface Protein 1 (MSP1)-Specific Antibodies

That Interfere with Parasite Growth In Vitro Can Inhibit MSP1 Processing, Merozoite Invasion, and Intracellular Parasite Development. *Infect. Immun.* **2012**, *80*, 1280−1287.

(42) Vagin, A.; Teplyakov, A. An approach to multi-copy search in molecular replacement. *Acta Crystallogr., Sect. D: Biol. Crystallogr.* **2000**, *56*, 1622−1624.

(43) Brannigan, J. A.; Smith, B. A.; Yu, Z.; Brzozowski, A. M.; Hodgkinson, M. R.; Maroof, A.; Price, H. P.; Meier, F.; Leatherbarrow, R. J.; Tate, E. W.; Smith, D. F.; Wilkinson, A. J. *N*-Myristoyltransferase from *Leishmania donovani*: Structural and Functional Characterisation of a Potential Drug Target for Visceral Leishmaniasis. *J. Mol. Biol.* **2010**, *396*, 985−999.

(44) Kabsch, W. XDS. *Acta Crystallogr., Sect. D: Biol. Crystallogr.* **2010**, *66*, 125−132.

(45) Evans, P. Scaling and assessment of data quality. *Acta Crystallogr., Sect. D: Biol. Crystallogr.* **2006**, *62*, 72−82.

(46) Winter, G. xia2: an expert system for macromolecular crystallography data reduction. *J. Appl. Crystallogr.* **2010**, *43*, 186−190.

(47) Murshudov, G. N.; Vagin, A. A.; Dodson, E. J. Refinement of Macromolecular Structures by the Maximum-Likelihood Method. *Acta Crystallogr., Sect. D: Biol. Crystallogr.* **1997**, *53*, 240−255.

(48) Emsley, P.; Lohkamp, B.; Scott, W. G.; Cowtan, K. Features and development of Coot. *Acta Crystallogr., Sect. D: Biol. Crystallogr.* **2010**, *66*, 486−501.